Chapter 4
Hybrid-Mixed Solid-Shell Element for Stress Analysis of Laminated Piezoelectric Shells through Higher-Order Theories

Gennady M. Kulikov, Svetlana V. Plotnikova, and Erasmo Carrera

Abstract A geometrically exact hybrid-mixed four-node piezoelectric solid-shell element by using the sampling surfaces (SaS) method is developed. The SaS formulation is based on choosing inside the layers the arbitrary number of SaS parallel to the middle surface and located at Chebyshev polynomial nodes in order to introduce the displacements and electric potentials of these surfaces as basic shell unknowns. The external surfaces and interfaces are also included into a set of SaS because of the variational formulation. Such a choice of unknowns with the consequent use of Lagrange polynomials in the through-thickness approximations of displacements, strains, electric potential and electric field leads to a very compact piezoelectric shell element formulation. To implement the efficient analytical integration throughout the element, the enhanced assumed natural strain (ANS) method is employed. The proposed hybrid-mixed four-node piezoelectric shell element is based on the Hu-Washizu variational equation and exhibits a superior performance in the case of coarse meshes. It could be useful for the three-dimensional (3D) stress analysis of thick and thin doubly-curved laminated piezoelectric shells since the SaS formulation gives the possibility to obtain the numerical solutions with a prescribed accuracy, which asymptotically approach the exact solutions of piezoelectricity as the number of SaS tends to infinity.

Gennady M. Kulikov · Svetlana V. Plotnikova
Laboratory of Intelligent Materials and Structures, Tambov State Technical University, Sovetskaya Street, 106, Tambov 392000, Russia
e-mail: gmkulikov@mail.ru

Erasmo Carrera
Department of Mechanical and Aerospace Engineering, Politecnico di Torino, Corso Duca degli Abbruzzi 24, 10129, Turin, Italy
e-mail: erasmo.carrera@polito.it

H. Altenbach et al. (eds.), *Analysis and Modelling of Advanced Structures and Smart Systems*, Advanced Structured Materials 81,
https://doi.org/10.1007/978-981-10-6895-9_4

4.1 Introduction

A large number of works has been carried out on 3D continuum-based finite elements (Sze and Yao, 2000; Sze et al, 2000; Lee et al, 2003; Zheng et al, 2004; Klinkel and Wagner, 2006, 2008; Kulikov and Plotnikova, 2008; Lentzen, 2009) that can handle the analysis of thin laminated piezoelectric shells satisfactorily. These elements are typically defined by two layers of nodes at the bottom and top surfaces with three translational and one electric degrees of freedom (DOF) per node and known as 6-parameter piezoelectric solid-shell elements because of the total number of translational DOF. Unfortunately, the 6-parameter solid-shell element formulation based on the complete 3D constitutive equations of piezoelectricity is deficient because thickness locking occurs. This is due to the fact that the linear displacement field in the thickness direction results in a constant transverse normal strain, which in turn causes artificial stiffening of the shell element in the case of non-vanishing Poisson's ratios. To prevent thickness locking, the 3D constitutive equations have to be modified employing the generalized plane stress conditions (Lee et al, 2003; Kulikov and Plotnikova, 2008). The hybrid stress method (Sze and Yao, 2000; Sze et al, 2000) in which the transverse normal stress is constant through the shell thickness and the enhanced assumed strain method in which the transverse normal strain is enriched in the thickness direction by a linear term (Zheng et al, 2004; Klinkel and Wagner, 2006, 2008; Lentzen, 2009) can be also utilized.

An efficient way of using the complete 3D constitutive equations for the analysis of piezoelectric shells is to employ the first-order equivalent single layer (ESL) theory with seven translational DOF (Kulikov and Plotnikova, 2010, 2011a). The 7-parameter ESL shell model is based on choosing six displacements and two electric potentials of the bottom and top surfaces and a transverse displacement of the middle surface as basic shell unknowns. Such a model is optimal with respect to the number of DOF. The more general 9-parameter ESL shell model is based on considering the external and middle surfaces and choosing the displacements and electric potentials of these surfaces as shell unknowns (Kulikov and Plotnikova, 2011b, 2015). Such choice of unknowns with the consequent use of Lagrange polynomials of the second order in the through-thickness approximations of displacements, strains, electric potential and electric field leads to a robust piezoelectric shell formulation. Moreover, this approach allows the derivation of the objective strain-displacement equations, which exactly represent all rigid-body shell motions in any convected curvilinear coordinate system. Taking into account that the displacement vectors of reference surfaces are resolved in the middle surface frame, the higher-order shell formulation with nine DOF is very promising for developing the exact geometry or geometrically exact (GeX) piezoelectric solid-shell elements. The term GeX implies that the parametrization of the middle surface is known a priori and, therefore, the coefficients of the first and second fundamental forms are taken exactly at element nodes.

Note that the above solid-shell elements (Sze and Yao, 2000; Sze et al, 2000; Lee et al, 2003; Zheng et al, 2004; Klinkel and Wagner, 2006, 2008; Kulikov and Plotnikova, 2008; Lentzen, 2009; Kulikov and Plotnikova, 2010, 2011a,b, 2015) do not describe properly the transverse stresses in a laminated piezoelectric shell.

To calculate them a post-processing stress recovery technique has to be employed. However, to evaluate the distribution of transverse stresses through the thickness of the laminated piezoelectric shell, higher-order layer-wise (LW) models have to be utilized. Robust GeX nine-node piezoelectric shell elements with a variable number of DOF per node have been developed in contributions (Carrera et al, 2011, 2014; Cinefra et al, 2015; Carrera and Valvano, 2017) through Carrera's unified formulation (Carrera, 1999, 2003). The shear and membrane locking phenomena (Carrera et al, 2014; Cinefra et al, 2015; Carrera and Valvano, 2017) are prevented by using the MITC technique (Bathe and Dvorkin, 1986; Bathe et al, 2003). These finite elements exhibit an excellent performance and can be recommended for the 3D stress analysis of piezoelectric shells. At the same time, Cinefra et al (2015) report that the piezoelectric shell element based on the fourth-order LW theory does not provide the continuity of the transverse normal stress and electric displacement on interfaces especially in the case of thin shells.

The present paper is intended to overcome the aforementioned difficulties and develop a piezoelectric solid-shell element that makes it possible to evaluate all stress and electric displacement components effectively for thick and very thin shells. To solve such a problem, the GeX four-node solid-shell element using the sampling surface (SaS) method (Kulikov and Plotnikova, 2013) is proposed. The SaS formulation is based on choosing inside the nth layer I_n not equally spaced surfaces $\Omega^{(n)1}$, $\Omega^{(n)2}$,..., $\Omega^{(n)I_n}$ parallel to the middle surface in order to introduce the displacements and electric potentials of these surfaces as basic shell variables, where $I_n \geq 3$. Such choice of unknowns with the consequent use of Lagrange polynomials of degree $I_n - 1$ in the assumed distributions of displacements, strains, electric potential and electric field through the thickness yields a very compact piezoelectric shell formulation. Recently, the SaS formulation has been employed to analyze analytically the electroelastic and thermoelectroelastic stress fields in laminated and functionally graded shells (Kulikov and Plotnikova, 2014; Kulikov et al, 2015; Kulikov and Plotnikova, 2017). However, the piezoelectric shell elements via the SaS technique have not been developed yet.

The origin of the SaS concept can be traced back to contributions (Kulikov, 2001; Kulikov and Carrera, 2008) in which three, four and five equally spaced SaS are utilized. The SaS formulation with an arbitrary number of equispaced SaS is considered in (Kulikov and Plotnikova, 2011d). The more general approach with the SaS located at Chebyshev polynomial nodes (roots of the Chebyshev polynomial) (Bakhvalov, 1977) was developed later (Kulikov and Plotnikova, 2013, 2014) because the SaS formulation with equispaced SaS does not work properly with the higher-order Lagrange interpolation. The use of the Chebyshev polynomial nodes improves significantly the behavior of the higher-degree Lagrange polynomials since such choice makes possible to minimize uniformly the error due to the Lagrange interpolation. This fact gives an opportunity to calculate the displacements and stresses with a prescribed accuracy employing the sufficiently large number of SaS. Thus, the solutions based on the SaS concept can asymptotically approach the 3D exact solutions of piezoelectricity as the number of SaS tends to infinity.

Here, the GeX hybrid-mixed four-node piezoelectric solid-shell element formulation is developed with the SaS located inside the layers at Chebyshev polynomial nodes (Kulikov and Plotnikova, 2013). To circumvent shear and membrane locking, the assumed interpolations of displacement-independent strains and stresses are utilized through the Hu-Washizu variational principle. Such an approach exhibits an excellent performance in the case of coarse mesh configurations and has computational advantages compared to conventional isoparametric hybrid-mixed piezoelectric solid-shell element formulations (Sze and Yao, 2000; Sze et al, 2000; Lee et al, 2003; Zheng et al, 2004; Klinkel and Wagner, 2006, 2008), because it reduces the computational cost of the numerical integration in the evaluation of the element stiffness matrix. This is due to the fact that all element matrices require only direct substitutions, i.e., no expensive numerical matrix inversion is needed. Second, the GeX four-node solid-shell element formulation is based on the effective analytical integration throughout the finite element by using the enhanced ANS method (Kulikov and Plotnikova, 2015, 2011c). The latter has a great meaning for the numerical modeling of doubly-curved shells with variable curvatures.

4.2 Sampling Surface Shell Formulation

Consider a laminated shell of the thickness h. Let the middle surface Ω be described by orthogonal curvilinear coordinates θ_1 and θ_2, which refer to the lines of principal curvatures of its surface. The coordinate θ_3 is oriented along the unit vector $\mathbf{e}_3(\theta_1, \theta_2)$ normal to the middle surface. We introduce the following notations: $\mathbf{e}_\alpha(\theta_1, \theta_2)$ are the orthonormal base vectors of the middle surface; $A_\alpha(\theta_1, \theta_2)$ are the coefficients of the first fundamental form; $k_\alpha(\theta_1, \theta_2)$ are the principal curvatures of the middle surface; $c_\alpha = 1 + k_\alpha\theta_3$ are the components of the shifter tensor; $c_\alpha^{(n)i_n}(\theta_1, \theta_2)$ are the components of the shifter tensor at SaS defined as

$$c_\alpha^{(n)i_n} = c_\alpha(\theta_3^{(n)i_n}) = 1 + k_\alpha\theta_3^{(n)i_n}, \tag{4.1}$$

where $\theta_3^{(n)i_n}$ are the transverse coordinates of the SaS inside the nth layer given by

$$\theta_3^{(n)1} = \theta_3^{[n-1]}, \quad \theta_3^{(n)I_n} = \theta_3^{[n]}, \tag{4.2}$$

$$\theta_3^{(n)m_n} = \frac{1}{2}(\theta_3^{[n-1]} + \theta_3^{[n]}) - \frac{1}{2}h_n \cos\left(\pi\frac{2m_n - 3}{2(I_n - 2)}\right), \tag{4.3}$$

in which $\theta_3^{[n-1]}$ and $\theta_3^{[n]}$ are the transverse coordinates of interfaces $\Omega^{[n-1]}$ and $\Omega^{[n]}$ depicted in Fig. 4.1; $h_n = \theta_3^{[n]} - \theta_3^{[n-1]}$ is the thickness of the nth layer. Here and in the following derivations, the index n identifies the correspondence of any quantity to the nth layer and runs from 1 to N, where N is the number of layers; $N_{\mathrm{SaS}} = \sum_n I_n - N + 1$ is the total number of SaS; the indices i_n and introduced later j_n, k_n identify the correspondence of any quantity to the SaS of the nth layer and run from 1 to I_n; the

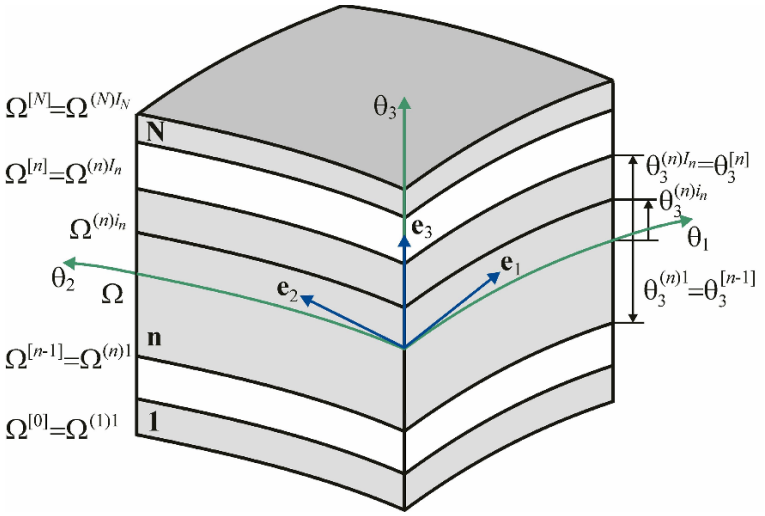

Fig. 4.1: Geometry of the laminated shell

index m_n identifies the belonging of any quantity to the inner SaS of the nth layer and runs from 2 to $I_n - 1$; Latin indices i, j, k, l range from 1 to 3; Greek indices α, β range from 1 to 2.

Remark 4.1. It is seen from Eq. (4.3) that the transverse coordinates of inner SaS $\theta_3^{(n)i_n}$ coincide with the coordinates of Chebyshev polynomial nodes This fact has a great meaning for the convergence of the SaS method

The through-thickness SaS approximations (Kulikov and Plotnikova, 2013) can be written as

$$\left[u_i^{(n)}\ \varepsilon_{ij}^{(n)}\ \sigma_{ij}^{(n)}\ \varphi^{(n)}\ E_i^{(n)}\right] = \sum_{i_n} L^{(n)i_n}\left[u_i^{(n)i_n}\ \varepsilon_{ij}^{(n)i_n}\ \sigma_{ij}^{(n)i_n}\ \varphi^{(n)i_n}\ E_i^{(n)i_n}\right], \tag{4.4}$$

where $u_i^{(n)}$, $\varepsilon_{ij}^{(n)}$, $\sigma_{ij}^{(n)}$, $\varphi^{(n)}$, $E_i^{(n)}$ are the displacements, strains, stresses, electric potential and electric field of the nth layer; $u_i^{(n)i_n}(\theta_1, \theta_2)$, $\varepsilon_{ij}^{(n)i_n}(\theta_1, \theta_2)$, $\sigma_{ij}^{(n)i_n}(\theta_1, \theta_2)$, $\varphi^{(n)i_n}(\theta_1, \theta_2)$ and $E_i^{(n)i_n}(\theta_1, \theta_2)$ are the displacements, strains, electric potential and electric field of SaS of the nth layer $\Omega^{(n)i_n}$; $L^{(n)i_n}(\theta_3)$ are the Lagrange basis polynomials of degree $I_n - 1$ related to the nth layer:

$$L^{(n)i_n} = \prod_{j_n \neq i_n} \frac{\theta_3 - \theta_3^{(n)j_n}}{\theta_3^{(n)i_n} - \theta_3^{(n)j_n}}. \tag{4.5}$$

In the orthonormal basis $\mathbf{e}_i$, the relations between strains and displacements of SaS of the nth layer are written as

$$2\varepsilon_{\alpha\beta}^{(n)i_n} = \frac{1}{c_\beta^{(n)i_n}}\lambda_{\alpha\beta}^{(n)i_n} + \frac{1}{c_\alpha^{(n)i_n}}\lambda_{\beta\alpha}^{(n)i_n},$$

$$2\varepsilon_{\alpha 3}^{(n)i_n} = \frac{1}{c_\alpha^{(n)i_n}}\lambda_{3\alpha}^{(n)i_n} + \beta_\alpha^{(n)i_n}, \quad \varepsilon_{33}^{(n)i_n} = \beta_3^{(n)i_n}, \tag{4.6}$$

where $\lambda_{i\alpha}^{(n)i_n}(\theta_1, \theta_2)$ are the strain parameters of SaS of the nth layer; $\beta_i^{(n)i_n}(\theta_1, \theta_2)$ are the values of the derivative of displacements with respect to thickness coordinate on SaS:

$$\lambda_{\alpha\alpha}^{(n)i_n} = \frac{1}{A_\alpha}u_{\alpha,\alpha}^{(n)i_n} + B_\alpha u_\beta^{(n)i_n} + k_\alpha u_3^{(n)i_n} \text{ for } \beta \neq \alpha,$$

$$\lambda_{\beta\alpha}^{(n)i_n} = \frac{1}{A_\alpha}u_{\beta,\alpha}^{(n)i_n} - B_\alpha u_\alpha^{(n)i_n} \text{ for } \beta \neq \alpha,$$

$$\lambda_{3\alpha}^{(n)i_n} = \frac{1}{A_\alpha}u_{3,\alpha}^{(n)i_n} - k_\alpha u_\alpha^{(n)i_n}, \quad B_\alpha = \frac{1}{A_\alpha A_\beta}A_{\alpha,\beta} \text{ for } \beta \neq \alpha, \tag{4.7}$$

$$\beta \tag{4.8}$$

where the symbol $(\ldots)_{,i}$ stands for the partial derivatives with respect to coordinates θ_i; $M^{(n)j_n} = L_{,3}^{(n)j_n}$ are the derivatives of Lagrange basis polynomials, which are calculated at the SaS as follows:

$$M^{(n)j_n}(\theta_3^{(n)i_n}) = \frac{1}{\theta_3^{(n)j_n} - \theta_3^{(n)i_n}} \prod_{k_n \neq i_n,\, j_n} \frac{\theta_3^{(n)i_n} - \theta_3^{(n)k_n}}{\theta_3^{(n)j_n} - \theta_3^{(n)k_n}} \text{ for } j_n \neq i_n,$$

$$M^{(n)i_n}(\theta_3^{(n)i_n}) = -\sum_{j_n \neq i_n} M^{(n)j_n}(\theta_3^{(n)i_n}). \tag{4.9}$$

In the orthonormal basis $\mathbf{e}_i$, the relations between the electric field and electric potentials of the SaS of the nth layer (Kulikov and Plotnikova, 2013) are expressed as

$$E_\alpha^{(n)i_n} = -\frac{1}{A_\alpha c_\alpha^{(n)i_n}}\varphi_{,\alpha}^{(n)i_n},$$

$$E_3^{(n)i_n} = -\sum_{j_n} M^{(n)j_n}(\theta_3^{(n)i_n})\varphi^{(n)j_n}. \tag{4.10}$$

4.3 Hu-Washizu Variational Equation

The proposed hybrid-mixed piezoelectric solid-shell element is based on the modified Hu-Washizu variational equation of piezoelectricity in which displacements, strains, stresses and electric potential are utilized as independent variables (Kulikov and Plotnikova, 2015):

$$\delta J = 0, \tag{4.11}$$

$$J = \iint\limits_{\Omega} \sum_{n} \int\limits_{\theta_3^{[n-1]}}^{\theta_3^{[n]}} \left[\frac{1}{2} \eta_{ij}^{(n)} C_{ijkl}^{(n)} \eta_{kl}^{(n)} - E_k^{(n)} e_{kij}^{(n)} \eta_{ij}^{(n)} - \frac{1}{2} E_i^{(n)} \epsilon_{ij}^{(n)} E_j^{(n)} \right.$$

$$\left. - \sigma_{ij}^{(n)} \left(\eta_{ij}^{(n)} - \varepsilon_{ij}^{(n)} \right) \right] dV - W, \tag{4.12}$$

where $dV = A_1 A_2 c_1 c_2 d\theta_1 d\theta_2 d\theta_3$ is the infinitesimal volume element; $\varepsilon_{ij}^{(n)}$ and $\eta_{ij}^{(n)}$ are the displacement-dependent and displacement-independent strains of the nth layer; $C_{ijkl}^{(n)}$, $e_{kij}^{(n)}$ and $\epsilon_{ij}^{(n)}$ are the elastic, piezoelectric and dielectric constants of the nth layer; W is the work done by external electromechanical loads. As usual, the summation on repeated Latin indices is implied.

Following the SaS technique (4.4), we introduce the next assumption of the hybrid-mixed solid-shell element formulation. Assume that the displacement-independent strains are distributed through the thickness of the nth layer by

$$\eta_{ij}^{(n)} = \sum_{i_n} L^{(n)i_n} \eta_{ij}^{(n)i_n}, \tag{4.13}$$

where $\eta_{ij}^{(n)i_n}(\theta_1, \theta_2)$ are the displacement-independent strains of SaS of the nth layer.

Substituting the through-thickness distributions (4.4) and (4.13) in Eq. (4.12) and introducing

$$\Lambda^{(n)i_n j_n} = \int\limits_{\theta_3^{[n-1]}}^{\theta_3^{[n]}} L^{(n)i_n} L^{(n)j_n} c_1 c_2 d\theta_3, \tag{4.14}$$

one can write the Hu-Washizu mixed functional in terms of SaS variables as

$$J = \iint\limits_{\Omega} \sum_{n} \sum_{i_n} \sum_{j_n} \Lambda^{(n)i_n j_n} \left[\frac{1}{2} (\boldsymbol{\eta}^{(n)i_n})^{\mathrm{T}} \mathbf{C}^{(n)} \boldsymbol{\eta}^{(n)j_n} - (\mathbf{E}^{(n)i_n})^{\mathrm{T}} \mathbf{e}^{(n)} \boldsymbol{\eta}^{(n)j_n} \right.$$

$$\left. - \frac{1}{2} (\mathbf{E}^{(n)i_n})^{\mathrm{T}} \boldsymbol{\epsilon}^{(n)} \mathbf{E}^{(n)j_n} - (\boldsymbol{\sigma}^{(n)i_n})^{\mathrm{T}} (\boldsymbol{\eta}^{(n)j_n} - \boldsymbol{\varepsilon}^{(n)j_n}) \right] A_1 A_2 d\theta_1 d\theta_2 - W, \tag{4.15}$$

where

$$\boldsymbol{\varepsilon}^{(n)i_n} = \left[\varepsilon_{11}^{(n)i_n} \; \varepsilon_{22}^{(n)i_n} \; \varepsilon_{33}^{(n)i_n} \; 2\varepsilon_{12}^{(n)i_n} \; 2\varepsilon_{13}^{(n)i_n} \; 2\varepsilon_{23}^{(n)i_n} \right]^{\mathrm{T}},$$

$$\boldsymbol{\eta}^{(n)i_n} = \left[\eta_{11}^{(n)i_n} \; \eta_{22}^{(n)i_n} \; \eta_{33}^{(n)i_n} \; 2\eta_{12}^{(n)i_n} \; 2\eta_{13}^{(n)i_n} \; 2\eta_{23}^{(n)i_n} \right]^{\mathrm{T}},$$

$$\boldsymbol{\sigma}^{(n)i_n} = \left[\sigma_{11}^{(n)i_n} \; \sigma_{22}^{(n)i_n} \; \sigma_{33}^{(n)i_n} \; \sigma_{12}^{(n)i_n} \; \sigma_{13}^{(n)i_n} \; \sigma_{23}^{(n)i_n} \right]^{\mathrm{T}},$$

$$\mathbf{E}^{(n)i_n} = \left[E_1^{(n)i_n} \; E_2^{(n)i_n} \; E_3^{(n)i_n} \right]^{\mathrm{T}},$$

$$\mathbf{C}^{(n)} = \begin{bmatrix} C^{(n)}_{1111} & C^{(n)}_{1122} & C^{(n)}_{1133} & C^{(n)}_{1112} & 0 & 0 \\ C^{(n)}_{2211} & C^{(n)}_{2222} & C^{(n)}_{2233} & C^{(n)}_{2212} & 0 & 0 \\ C^{(n)}_{3311} & C^{(n)}_{3322} & C^{(n)}_{3333} & C^{(n)}_{3312} & 0 & 0 \\ C^{(n)}_{1211} & C^{(n)}_{1222} & C^{(n)}_{1233} & C^{(n)}_{1212} & 0 & 0 \\ 0 & 0 & 0 & 0 & C^{(n)}_{1313} & C^{(n)}_{1323} \\ 0 & 0 & 0 & 0 & C^{(n)}_{2313} & C^{(n)}_{2323} \end{bmatrix},$$

$$\mathbf{e}^{(n)} = \begin{bmatrix} 0 & 0 & 0 & 0 & e^{(n)}_{113} & e^{(n)}_{123} \\ 0 & 0 & 0 & 0 & e^{(n)}_{213} & e^{(n)}_{223} \\ e^{(n)}_{311} & e^{(n)}_{322} & e^{(n)}_{333} & e^{(n)}_{312} & 0 & 0 \end{bmatrix},$$

$$\boldsymbol{\epsilon}^{(n)} = \begin{bmatrix} \epsilon^{(n)}_{11} & \epsilon^{(n)}_{12} & 0 \\ \epsilon^{(n)}_{21} & \epsilon^{(n)}_{22} & 0 \\ 0 & 0 & \epsilon^{(n)}_{33} \end{bmatrix}. \tag{4.16}$$

4.4 Hybrid-Mixed Solid-Shell Element Formulation

The finite element formulation is based on a simple interpolation of the shell via GeX four-node piezoelectric solid-shell elements

$$u_i^{(n)i_n} = \sum_r N_r u_{ir}^{(n)i_n}, \quad \varphi^{(n)i_n} = \sum_r N_r \varphi_r^{(n)i_n}, \tag{4.17}$$

where $N_r(\xi_1, \xi_2)$ are the bilinear shape functions of the element; $u_{ir}^{(n)i_n}$ and $\varphi_r^{(n)i_n}$ are the displacements and electric potentials of SaS $\Omega^{(n)i_n}$ at element nodes; ξ_1, ξ_2 are the normalized curvilinear coordinates θ_1, θ_2 (Fig. 4.2); the nodal index r runs from 1 to 4.

To implement the efficient analytical integration throughout the finite element, the enhanced ANS method (Kulikov and Plotnikova, 2011c) is adopted

$$\boldsymbol{\varepsilon}^{(n)i_n} = \sum_r N_r \boldsymbol{\varepsilon}_r^{(n)i_n}, \tag{4.18}$$

$$\boldsymbol{\varepsilon}_r^{(n)i_n} = \left[\varepsilon_{11r}^{(n)i_n} \ \varepsilon_{22r}^{(n)i_n} \ \varepsilon_{33r}^{(n)i_n} \ 2\varepsilon_{12r}^{(n)i_n} \ 2\varepsilon_{13r}^{(n)i_n} \ 2\varepsilon_{23r}^{(n)i_n}\right]^{\mathrm{T}},$$

$$\mathbf{E}^{(n)i_n} = \sum_r N_r \mathbf{E}_r^{(n)i_n}, \tag{4.19}$$

$$\mathbf{E}_r^{(n)i_n} = \left[E_{1r}^{(n)i_n} \ E_{2r}^{(n)i_n} \ E_{3r}^{(n)i_n}\right]^{\mathrm{T}},$$

where $\varepsilon_{ijr}^{(n)i_n}$ and $E_{ir}^{(n)i_n}$ are the strains and electric field of SaS of the nth layer at element nodes.

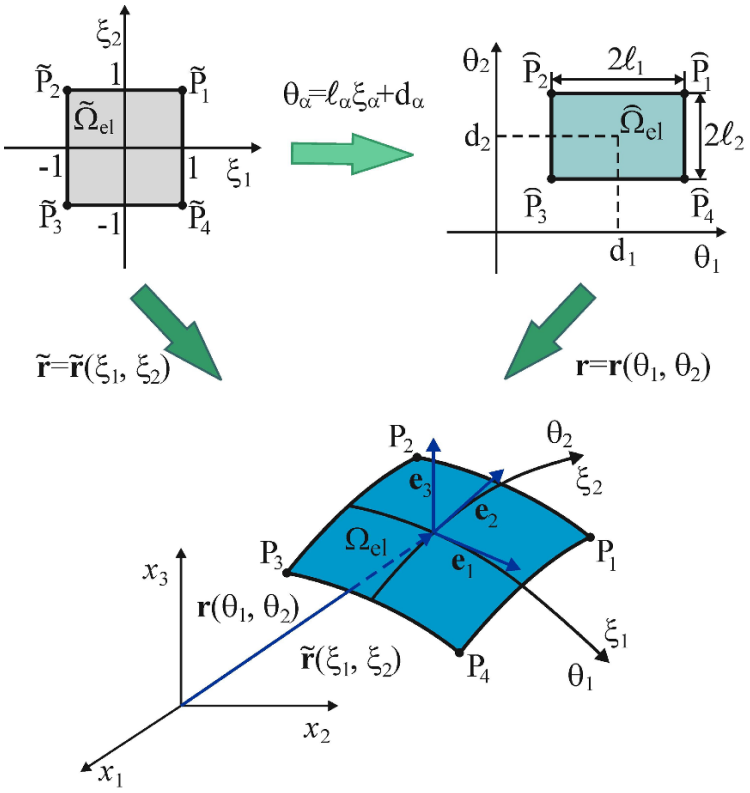

Fig. 4.2: Biunit square in (ξ_1,ξ_2)-space mapped into the middle surface of the GeX four-node solid-shell element in (x_1,x_2,x_3)-space

Remark 4.2. The main idea of such approach can be traced back to the ANS method developed by many scientists for the isoparametric finite element formulation (Bathe and Dvorkin, 1986; Hughes and Tezduyar, 1981; Macneal, 1982; Park and Stanley, 1986; Ko et al, 2017; Betsch and Stein, 1995). In contrast with above formulation, we treat the term ANS in a broader sense. In the proposed GeX four-node solid-shell element formulation, all components of the displacement-dependent strain tensor and electric field are assumed to vary bilinearly throughout the biunit square in (ξ_1, ξ_2)-space. This implies that instead of the expected *non-linear* interpolations due to Eqs. (4.6), (4.7) and (4.10) the more suitable *bilinear* interpolations (4.18) and (4.19) are utilized.

The strain vectors of the SaS at element nodes can be expressed as

$$\boldsymbol{\varepsilon}_r^{(n)i_n} = \mathbf{B}_{ur}^{(n)i_n}\mathbf{U}, \tag{4.20}$$

where $\mathbf{B}_{ur}^{(n)i_n}$ are the constant inside the finite element matrices of order $6\times 12N_{\mathrm{SaS}}$; $\mathbf{U}$ is the element displacement vector given by

$$\mathbf{U} = \left[\mathbf{U}_1^{\mathrm{T}}\,\mathbf{U}_2^{\mathrm{T}}\,\mathbf{U}_3^{\mathrm{T}}\,\mathbf{U}_4^{\mathrm{T}}\right]^{\mathrm{T}},$$

$$\mathbf{U}_r = \left[\left(\mathbf{u}_r^{[0]}\right)^{\mathrm{T}}\left(\mathbf{u}_r^{(1)2}\right)^{\mathrm{T}}\ldots\left(\mathbf{u}_r^{(1)I_1-1}\right)^{\mathrm{T}}\left(\mathbf{u}_r^{[1]}\right)^{\mathrm{T}}\left(\mathbf{u}_r^{(2)2}\right)^{\mathrm{T}}\right.$$

$$\left.\ldots\left(\mathbf{u}_r^{(N-1)I_{N-1}-1}\right)^{\mathrm{T}}\left(\mathbf{u}_r^{[N-1]}\right)^{\mathrm{T}}\left(\mathbf{u}_r^{(N)2}\right)^{\mathrm{T}}\ldots\left(\mathbf{u}_r^{(N)I_N-1}\right)^{\mathrm{T}}\left(\mathbf{u}_r^{[N]}\right)^{\mathrm{T}}\right]^{\mathrm{T}},$$

$$\mathbf{u}_r^{[m]} = \left[u_{1r}^{[m]}\,u_{2r}^{[m]}\,u_{3r}^{[m]}\right]^{\mathrm{T}},\quad \mathbf{u}_r^{(n)m_n} = \left[u_{1r}^{(n)m_n}\,u_{2r}^{(n)m_n}\,u_{3r}^{(n)m_n}\right]^{\mathrm{T}}, \tag{4.21}$$

where $u_{ir}^{[m]}$ are the displacements of external surfaces and interfaces at element nodes ($m = 0, 1, ..., N$).

The electric field vectors of SaS at element nodes are

$$\mathbf{E}_r^{(n)i_n} = -\mathbf{B}_{\varphi r}^{(n)i_n}\boldsymbol{\Phi}, \tag{4.22}$$

where $\mathbf{B}_{\varphi r}^{(n)i_n}$ are the constant inside the finite element matrices of order $3\times 4N_{\mathrm{SaS}}$; $\boldsymbol{\Phi}$ is the element electric field vector defined as

$$\boldsymbol{\Phi} = \left[\boldsymbol{\Phi}_1^{\mathrm{T}}\,\boldsymbol{\Phi}_2^{\mathrm{T}}\,\boldsymbol{\Phi}_3^{\mathrm{T}}\,\boldsymbol{\Phi}_4^{\mathrm{T}}\right]^{\mathrm{T}},$$

$$\boldsymbol{\Phi}_r = \left[\varphi_r^{[0]}\,\varphi_r^{(1)2}\ldots\varphi_r^{(1)I_1-1}\,\varphi_r^{[1]}\,\varphi_r^{(2)2}\right.$$

$$\left.\ldots\,\varphi_r^{(N-1)I_{N-1}-1}\,\varphi_r^{[N-1]}\,\varphi_r^{(N)2}\ldots\,\varphi_r^{(N)I_N-1}\,\varphi_r^{[N]}\right]^{\mathrm{T}}, \tag{4.23}$$

where $\varphi_r^{[m]}$ are the electric potentials of external surfaces and interfaces at element nodes.

From a computational point of view, it is convenient to write the ANS interpolation (4.18) in the following form:

$$\boldsymbol{\varepsilon}^{(n)i_n} = \sum_{r_1,r_2}(\xi_1)^{r_1}(\xi_2)^{r_2}\,\boldsymbol{\varepsilon}_{r_1r_2}^{(n)i_n},\qquad \boldsymbol{\varepsilon}_{r_1r_2}^{(n)i_n} = \mathbf{B}_{ur_1r_2}^{(n)i_n}\mathbf{U}, \tag{4.24}$$

where

$$\boldsymbol{\varepsilon}_{r_1r_2}^{(n)i_n} = \left[\varepsilon_{11r_1r_2}^{(n)i_n}\,\varepsilon_{22r_1r_2}^{(n)i_n}\,\varepsilon_{33r_1r_2}^{(n)i_n}\,2\varepsilon_{12r_1r_2}^{(n)i_n}\,2\varepsilon_{13r_1r_2}^{(n)i_n}\,2\varepsilon_{23r_1r_2}^{(n)i_n}\right]^{\mathrm{T}},$$

$$\mathbf{B}_{u00}^{(n)i_n} = \frac{1}{4}\left(\mathbf{B}_{u1}^{(n)i_n} + \mathbf{B}_{u2}^{(n)i_n} + \mathbf{B}_{u3}^{(n)i_n} + \mathbf{B}_{u4}^{(n)i_n}\right),$$

$$\mathbf{B}_{u01}^{(n)i_n} = \frac{1}{4}\left(\mathbf{B}_{u1}^{(n)i_n} + \mathbf{B}_{u2}^{(n)i_n} - \mathbf{B}_{u3}^{(n)i_n} - \mathbf{B}_{u4}^{(n)i_n}\right),$$

$$\mathbf{B}_{u10}^{(n)i_n} = \frac{1}{4}\left(\mathbf{B}_{u1}^{(n)i_n} - \mathbf{B}_{u2}^{(n)i_n} - \mathbf{B}_{u3}^{(n)i_n} + \mathbf{B}_{u4}^{(n)i_n}\right),$$

$$\mathbf{B}_{u11}^{(n)i_n} = \frac{1}{4}\left(\mathbf{B}_{u1}^{(n)i_n} - \mathbf{B}_{u2}^{(n)i_n} + \mathbf{B}_{u3}^{(n)i_n} - \mathbf{B}_{u4}^{(n)i_n}\right). \tag{4.25}$$

Here, and below the indices r_1 and r_2 run from 0 to 1. The same concerns the ANS interpolation (4.19), that is,

$$\mathbf{E}^{(n)i_n} = \sum_{r_1,r_2} (\xi_1)^{r_1} (\xi_2)^{r_2} \mathbf{E}_{r_1 r_2}^{(n)i_n}, \qquad \text{with} \qquad \mathbf{E}_{r_1 r_2}^{(n)i_n} = -\mathbf{B}_{\varphi\, r_1 r_2}^{(n)i_n} \boldsymbol{\Phi}, \tag{4.26}$$

where

$$\begin{aligned}
\mathbf{E}_{r_1 r_2}^{(n)i_n} &= \left[E_{1 r_1 r_2}^{(n)i_n}\ E_{2 r_1 r_2}^{(n)i_n}\ E_{3 r_1 r_2}^{(n)i_n}\right]^{\mathrm{T}},\\
\mathbf{B}_{\varphi 00}^{(n)i_n} &= \frac{1}{4}\left(\mathbf{B}_{\varphi 1}^{(n)i_n} + \mathbf{B}_{\varphi 2}^{(n)i_n} + \mathbf{B}_{\varphi 3}^{(n)i_n} + \mathbf{B}_{\varphi 4}^{(n)i_n}\right),\\
\mathbf{B}_{\varphi 01}^{(n)i_n} &= \frac{1}{4}\left(\mathbf{B}_{\varphi 1}^{(n)i_n} + \mathbf{B}_{\varphi 2}^{(n)i_n} - \mathbf{B}_{\varphi 3}^{(n)i_n} - \mathbf{B}_{\varphi 4}^{(n)i_n}\right),\\
\mathbf{B}_{\varphi 10}^{(n)i_n} &= \frac{1}{4}\left(\mathbf{B}_{\varphi 1}^{(n)i_n} - \mathbf{B}_{\varphi 2}^{(n)i_n} - \mathbf{B}_{\varphi 3}^{(n)i_n} + \mathbf{B}_{\varphi 4}^{(n)i_n}\right),\\
\mathbf{B}_{\varphi 11}^{(n)i_n} &= \frac{1}{4}\left(\mathbf{B}_{\varphi 1}^{(n)i_n} - \mathbf{B}_{\varphi 2}^{(n)i_n} + \mathbf{B}_{\varphi 3}^{(n)i_n} - \mathbf{B}_{\varphi 4}^{(n)i_n}\right).
\end{aligned} \tag{4.27}$$

To overcome shear and membrane locking and introduce no spurious zero energy modes, the robust displacement-independent strain and stress interpolations are utilized:

$$\boldsymbol{\eta}^{(n)i_n} = \sum_{r_1+r_2<2} (\xi_1)^{r_1} (\xi_2)^{r_2} \mathbf{Q}_{r_1 r_2} \boldsymbol{\eta}_{r_1 r_2}^{(n)i_n}, \tag{4.28}$$

$$\begin{aligned}
\boldsymbol{\eta}_{00}^{(n)i_n} &= \left[\psi_1^{(n)i_n}\ \psi_2^{(n)i_n}\ \psi_3^{(n)i_n}\ \psi_4^{(n)i_n}\ \psi_5^{(n)i_n}\ \psi_6^{(n)i_n}\right]^{\mathrm{T}},\\
\boldsymbol{\eta}_{01}^{(n)i_n} &= \left[\psi_7^{(n)i_n}\ \psi_9^{(n)i_n}\ \psi_{11}^{(n)i_n}\right]^{\mathrm{T}}, \quad \boldsymbol{\eta}_{10}^{(n)i_n} = \left[\psi_8^{(n)i_n}\ \psi_{10}^{(n)i_n}\ \psi_{12}^{(n)i_n}\right]^{\mathrm{T}},
\end{aligned}$$

$$\boldsymbol{\sigma}^{(n)i_n} = \sum_{r_1+r_2<2} (\xi_1)^{r_1} (\xi_2)^{r_2} \mathbf{Q}_{r_1 r_2} \boldsymbol{\sigma}_{r_1 r_2}^{(n)i_n}, \tag{4.29}$$

$$\begin{aligned}
\boldsymbol{\sigma}_{00}^{(n)i_n} &= \left[\mu_1^{(n)i_n}\ \mu_2^{(n)i_n}\ \mu_3^{(n)i_n}\ \mu_4^{(n)i_n}\ \mu_5^{(n)i_n}\ \mu_6^{(n)i_n}\right]^{\mathrm{T}},\\
\boldsymbol{\sigma}_{01}^{(n)i_n} &= \left[\mu_7^{(n)i_n}\ \mu_9^{(n)i_n}\ \mu_{11}^{(n)i_n}\right]^{\mathrm{T}}, \quad \boldsymbol{\sigma}_{10}^{(n)i_n} = \left[\mu_8^{(n)i_n}\ \mu_{10}^{(n)i_n}\ \mu_{12}^{(n)i_n}\right]^{\mathrm{T}},
\end{aligned}$$

where $\mathbf{Q}_{r_1 r_2}$ are the projective matrices given by

$$\mathbf{Q}_{00} = \begin{bmatrix} 1&0&0&0&0&0\\ 0&1&0&0&0&0\\ 0&0&1&0&0&0\\ 0&0&0&1&0&0\\ 0&0&0&0&1&0\\ 0&0&0&0&0&1 \end{bmatrix}, \quad \mathbf{Q}_{01} = \begin{bmatrix} 1&0&0\\ 0&0&0\\ 0&1&0\\ 0&0&0\\ 0&0&1\\ 0&0&0 \end{bmatrix}, \quad \mathbf{Q}_{10} = \begin{bmatrix} 0&0&0\\ 1&0&0\\ 0&1&0\\ 0&0&0\\ 0&0&0\\ 0&0&1 \end{bmatrix}. \tag{4.30}$$

Remark 4.3. The assumed interpolations (4.28) and (4.29) provide a correct rank of the element stiffness matrix.

Substituting interpolations (4.17), (4.24), (4.26), (4.28) and (4.29) in the Hu-Washizu variational equation (4.11) and (4.15), replacing the metric product A_1A_2 in surface integrals by its value at the element center and integrating analytically throughout the finite element, the following equilibrium equations of the GeX hybrid-mixed four-node solid-shell element are obtained:

$$\boldsymbol{\eta}_{r_1r_2}^{(n)i_n} = \mathbf{Q}_{r_1r_2}^{\mathrm{T}}\mathbf{B}_{ur_1r_2}^{(n)i_n}\mathbf{U} \;\text{ for }\; r_1+r_2<2, \tag{4.31}$$

$$\boldsymbol{\sigma}_{r_1r_2}^{(n)i_n} = \mathbf{Q}_{r_1r_2}^{\mathrm{T}}\left(\mathbf{C}^{(n)}\mathbf{Q}_{r_1r_2}\boldsymbol{\eta}_{r_1r_2}^{(n)i_n} + (\mathbf{e}^{(n)})^{\mathrm{T}}\mathbf{B}_{\varphi r_1r_2}^{(n)i_n}\boldsymbol{\Phi}\right) \;\text{ for }\; r_1+r_2<2, \tag{4.32}$$

$$\sum_n\sum_{i_n}\sum_{j_n}\Lambda^{(n)i_nj_n}\sum_{r_1+r_2<2}\frac{1}{3^{r_1+r_2}}(\mathbf{B}_{ur_1r_2}^{(n)i_n})^{\mathrm{T}}\mathbf{Q}_{r_1r_2}\boldsymbol{\sigma}_{r_1r_2}^{(n)j_n} = \mathbf{F}_u, \tag{4.33}$$

$$\sum_n\sum_{i_n}\sum_{j_n}\Lambda^{(n)i_nj_n}\sum_{r_1+r_2<2}\frac{1}{3^{r_1+r_2}}(\mathbf{B}_{\varphi r_1r_2}^{(n)i_n})^{\mathrm{T}}\left(\mathbf{e}^{(n)}\mathbf{Q}_{r_1r_2}\boldsymbol{\eta}_{r_1r_2}^{(n)j_n} - \boldsymbol{\epsilon}^{(n)}\mathbf{B}_{\varphi r_1r_2}^{(n)j_n}\boldsymbol{\Phi}\right) = \mathbf{F}_\varphi, \tag{4.34}$$

where $\mathbf{F}_u$ and $\mathbf{F}_\varphi$ are the element-wise mechanical and electric surface vectors.

Eliminating vectors $\boldsymbol{\eta}_{r_1r_2}^{(n)i_n}$ and $\boldsymbol{\sigma}_{r_1r_2}^{(n)i_n}$ from Eqs. (4.31)-(4.34), one arrives at the system of linear equations

$$\begin{bmatrix}\mathbf{K}_{uu} & \mathbf{K}_{u\varphi}\\ \mathbf{K}_{\varphi u} & \mathbf{K}_{\varphi\varphi}\end{bmatrix}\begin{bmatrix}\mathbf{U}\\ \boldsymbol{\Phi}\end{bmatrix} = \begin{bmatrix}\mathbf{F}_u\\ \mathbf{F}_\varphi\end{bmatrix}, \tag{4.35}$$

where $\mathbf{K}_{uu}$, $\mathbf{K}_{u\varphi}$, $\mathbf{K}_{\varphi u} = \mathbf{K}_{u\varphi}^{\mathrm{T}}$ and $\mathbf{K}_{\varphi\varphi}$ are the mechanical, piezoelectric and dielectric stiffness matrices defined as

$$\mathbf{K}_{uu} = \sum_n\sum_{i_n}\sum_{j_n}\Lambda^{(n)i_nj_n}\sum_{r_1+r_2<2}\frac{1}{3^{r_1+r_2}}\left(\mathbf{B}_{ur_1r_2}^{(n)i_n}\right)^{\mathrm{T}}\mathbf{Q}_{r_1r_2}\mathbf{Q}_{r_1r_2}^{\mathrm{T}}\mathbf{C}^{(n)}\mathbf{Q}_{r_1r_2}\mathbf{Q}_{r_1r_2}^{\mathrm{T}}\mathbf{B}_{ur_1r_2}^{(n)j_n},$$

$$\mathbf{K}_{u\varphi} = \sum_n\sum_{i_n}\sum_{j_n}\Lambda^{(n)i_nj_n}\sum_{r_1+r_2<2}\frac{1}{3^{r_1+r_2}}\left(\mathbf{B}_{ur_1r_2}^{(n)i_n}\right)^{\mathrm{T}}\mathbf{Q}_{r_1r_2}\mathbf{Q}_{r_1r_2}^{\mathrm{T}}(\mathbf{e}^{(n)})^{\mathrm{T}}\mathbf{B}_{\varphi r_1r_2}^{(n)j_n},$$

$$\mathbf{K}_{\varphi\varphi} = -\sum_n\sum_{i_n}\sum_{j_n}\Lambda^{(n)i_nj_n}\sum_{r_1+r_2<2}\frac{1}{3^{r_1+r_2}}\left(\mathbf{B}_{\varphi r_1r_2}^{(n)i_n}\right)^{\mathrm{T}}\boldsymbol{\epsilon}^{(n)}\mathbf{B}_{\varphi r_1r_2}^{(n)j_n}. \tag{4.36}$$

Remark 4.4. It is worth noting that all stiffness matrices are evaluated without the expensive numerical matrix inversion that is impossible in available isoparametric hybrid-mixed finite element formulations.

4.5 Numerical Examples

The performance of the developed GeX four-node piezoelectric solid-shell element denoted by GeXPS4 element is evaluated with the help of several exact solutions of piezoelectricity extracted from the literature (Heyliger, 1997; Chen et al, 2001).

4.5.1 Three-Layer Piezoelectric Cylindrical Shell

Consider a simply supported three-layer cylindrical shell with equal ply thicknesses under the imposed transverse deformation on the top surface

$$u_3^+ = u_0 \sin \frac{\pi\theta_1}{L} \cos 2\theta_2, \tag{4.37}$$

where L is the length of the shell and $u_0 = 10^{-8}$ m. The both outer layers are composed of PZT-4 with the material properties presented in Table 4.1 and Heyliger (1997). The middle layer is made of fictitious material (Heyliger, 1997) with elastic constants exactly half of PZT-4 and the piezoelectric and dielectric constants exactly double of those of PZT-4. The bottom and top surfaces are assumed to be electrically grounded and traction free.

Table 4.1: Elastic, piezoelectric and dielectric properties of materials*

Material	PZT-4 (Heyliger, 1997)	PZT-4 (Dunn and Taya, 1994)	$BaTiO_3$ (Dunn and Taya, 1994)
C_{1111}, GPa	139.0	139.0	150.0
C_{2222}, GPa	139.0	139.0	150.0
C_{3333}, GPa	115.0	115.0	146.0
C_{1122}, GPa	77.8	77.8	66.0
C_{1133}, GPa	74.3	74.3	66.0
C_{2233}, GPa	74.3	74.3	66.0
C_{1313}, GPa	25.6	25.6	44.0
C_{2323}, GPa	25.6	25.6	44.0
C_{1212}, GPa	30.6	30.6	42.0
e_{311}, C/m^2	-5.2	-5.2	-4.35
e_{322}, C/m^2	-5.2	-5.2	-4.35
e_{333}, C/m^2	15.08	15.1	17.5
e_{113}, C/m^2	12.72	12.7	11.4
e_{223}, C/m^2	12.72	12.7	11.4
ϵ_{11}/ϵ_0	1475	730	1115
ϵ_{22}/ϵ_0	1475	730	1115
ϵ_{33}/ϵ_0	1300	635	1260

* Vacuum permittivity ϵ_0=8.854 pF/m

Due to symmetry of the problem, only one octant of the shell ($L/2 \le \theta_1 \le L$, $0 \le \theta_2 \le \pi/2$) is modeled by a regular mesh consisting of 48×96 GeXPS4 elements. To compare the results with the exact solution of Heyliger (1997), we take $L = R^+ = 0.01$ m and introduce the scaled variables as functions of the dimensionless thickness coordinate as follows:

$$\begin{aligned}
\bar{u}_1 &= 10^{11} \times u_1(L, 0, z), \quad \bar{u}_3 = 10^{11} \times u_3(L/2, 0, z), \\
\bar{\sigma}_{11} &= 10^{-3} \times \sigma_{11}(L/2, 0, z), \quad \bar{\sigma}_{22} = 10^{-3} \times \sigma_{22}(L/2, 0, z), \\
\bar{\sigma}_{13} &= 10^{-3} \times \sigma_{13}(L, 0, z), \quad \bar{\sigma}_{23} = 10^{-3} \times \sigma_{23}(L/2, \pi/4, z), \\
\bar{\sigma}_{33} &= 10^{-3} \times \sigma_{33}(L/2, 0, z), \\
\bar{\varphi} &= \varphi(L/2, 0, z), \quad \bar{D}_3 = 10^{6} \times D_3(L/2, 0, z), \quad z = \theta_3/h,
\end{aligned} \tag{4.38}$$

where R^+ is the radius of the top cylindrical surface.

Tables 4.2 and 4.3 list the results of the convergence study due to increasing the number of SaS I_n inside each layer for two values of the slenderness ratio $S = R^+/h$. A comparison with the exact SaS solution (Kulikov and Plotnikova, 2013) is also given. Fig. 4.3 shows the distributions of displacements, transverse stresses, electric potential and electric displacement through the thickness for different slenderness ratios by taking five SaS for each layer. These results demonstrate convincingly the high potential of the proposed GeX hybrid-mixed solid-shell element formulation. This is due to the facts that the boundary conditions on external surfaces for the transverse stresses and the continuity conditions on interfaces for the transverse stresses and electric displacement are satisfied for thick and thin shells properly.

The results of the convergence study due to mesh refinement are presented in Fig. 4.4. The analytical answer is provided by the exact SaS solution (Kulikov and Plotnikova, 2013). In this study, we consider five regular meshes with 3×6, 6×12, 12×24, 24×48 and 48×96 finite elements, which are characterized by the mesh parameter k running from 1 to 5. It is seen that the GeXPS4 element behaves well even in the case of coarse meshes except for the transverse normal stress for thin shells.

Table 4.2: Results for a three-layer cylindrical shell with $S = 2$ under mechanical loading

I_n	$\bar{u}_1(-0.5)$	$\bar{u}_3(-0.5)$	$\bar{\varphi}(0)$	$\bar{\sigma}_{22}(-0.5)$	$\bar{\sigma}_{13}(0)$	$\bar{\sigma}_{23}(0)$	$\bar{\sigma}_{33}(0)$	$\bar{D}_3(0)$
3	-251.6	740.2	2.849	-136.3	-56.80	-40.70	40.48	15.22
4	-254.6	742.2	2.851	-131.2	-57.71	-40.98	42.50	16.11
5	-254.3	742.1	2.851	-127.9	-57.57	-41.20	42.23	15.98
Exact	-254.3	742.1	2.851	-127.7	-57.59	-41.21	42.25	15.98

Next, we study the same three-layer piezoelectric cylindrical shell subjected to electric loading on the top surface whereas the bottom surface is electrically grounded

$$\varphi^- = 0, \quad \varphi^+ = \varphi_0 \sin \frac{\pi \theta_1}{L} \cos 2\theta_2, \tag{4.39}$$

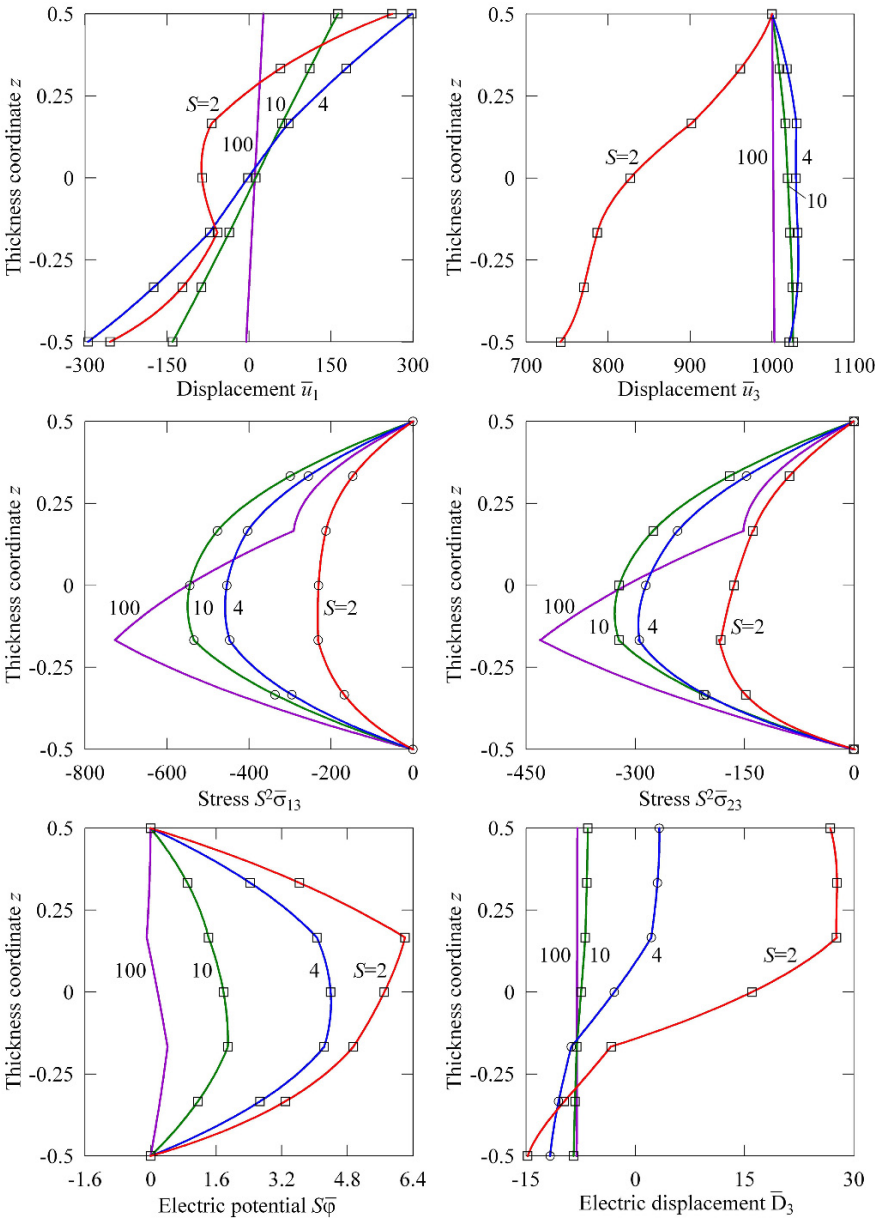

Fig. 4.3: Through-thickness distributions of displacements, transverse shear stresses, electric potential and electric displacement for a three-layer cylindrical shell subjected to mechanical loading for $I_1 = I_2 = I_3 = 5$: GeXPS4 element (—), exact SaS solution (Kulikov and Plotnikova, 2013) (∘) and Heyliger's exact 3D solution (Heyliger, 1997) (□)

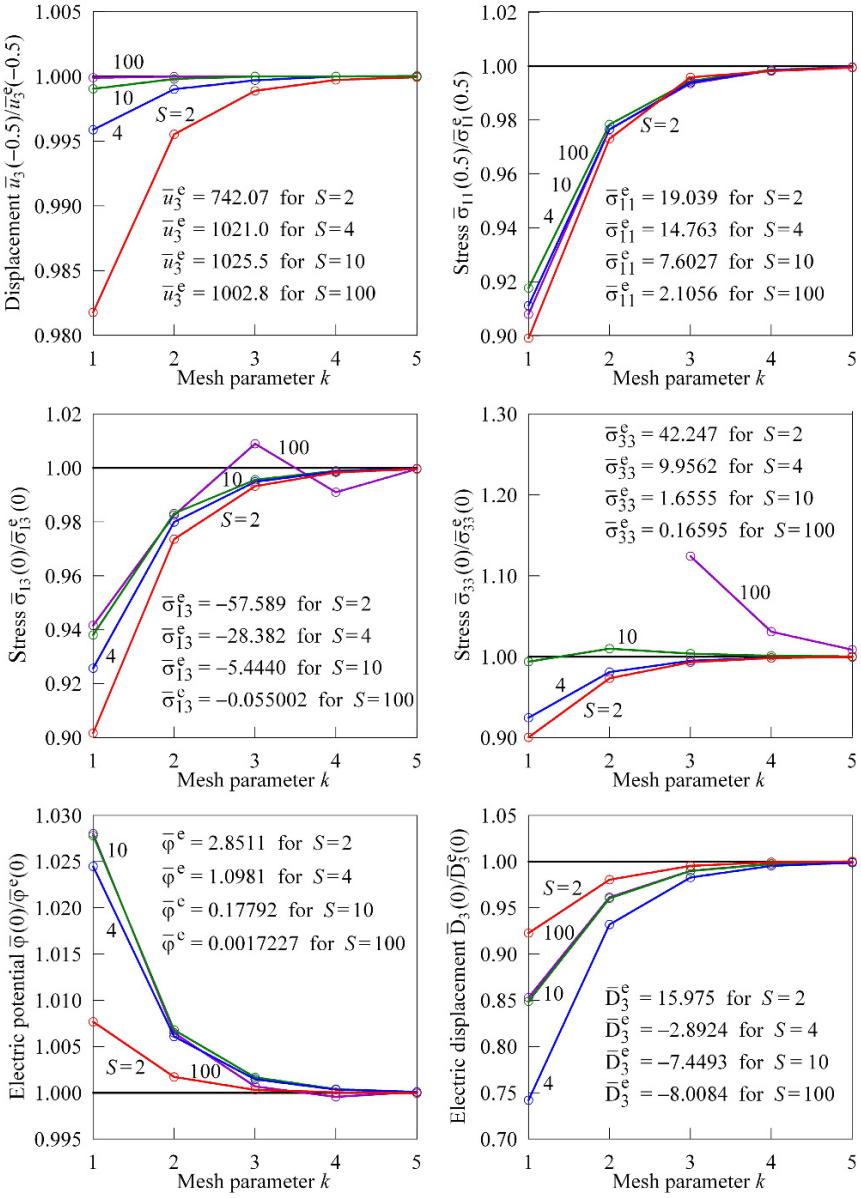

Fig. 4.4: Convergence study due to mesh refinement for a three-layer cylindrical shell subjected to mechanical loading for $I_1 = I_2 = I_3 = 5$; the reference solution (—) is provided by the exact SaS solution (Kulikov and Plotnikova, 2013)

Table 4.3: Results for a three-layer cylindrical shell with $S = 10$ under mechanical loading

I_n	$\bar{u}_1(-0.5)$	$\bar{u}_3(-0.5)$	$\bar{\varphi}(0)$	$\bar{\sigma}_{22}(-0.5)$	$\bar{\sigma}_{13}(0)$	$\bar{\sigma}_{23}(0)$	$\bar{\sigma}_{33}(0)$	$\bar{D}_3(0)$
3	-139.7	1026.	0.1780	-1.784	-5.352	-3.168	1.691	-7.452
4	-139.7	1026.	0.1779	-1.591	-5.445	-3.216	1.659	-7.444
5	-139.7	1026.	0.1779	-1.574	-5.443	-3.220	1.656	-7.445
Exact	-139.7	1026.	0.1779	-1.564	-5.440	-3.221	1.656	-7.449

where $\varphi_0 = 10\,\mathrm{V}$. The external surfaces are assumed to be traction free. Here, again one octant of the shell is modeled by a regular mesh with 48×96 GeXPS4 elements.

Table 4.4 lists the results of the convergence study for the moderately thick shell by increasing the number of SaS I_n inside each layer. The obtained results are compared with the exact SaS solution (Kulikov and Plotnikova, 2013). Figure 4.5 shows the through-thickness distributions of displacements, transverse stresses, electric potential and electric displacement (4.38) for different slenderness ratios S by choosing five SaS for each layer. It is seen that the boundary conditions on bottom and top surfaces and the continuity conditions at interfaces for transverse stresses and electric displacement are satisfied again correctly.

Table 4.4: Results for a three-layer cylindrical shell with $S = 10$ under electric loading

I_n	$\bar{u}_1(-0.5)$	$\bar{u}_3(-0.5)$	$\bar{\varphi}(0)$	$\bar{\sigma}_{11}(-0.5)$	$\bar{\sigma}_{13}(0)$	$\bar{\sigma}_{23}(0)$	$\bar{\sigma}_{33}(0)$	$\bar{D}_3(0)$
3	216.2	1664.	5.239	-12.12	-9.910	-5.866	-1.527	-221.2
4	216.1	1664.	5.239	-12.14	-10.11	-5.979	-1.535	-221.1
5	216.1	1664.	5.239	-12.14	-10.11	-5.977	-1.535	-221.1
Exact	216.2	1665.	5.239	-12.15	-10.11	-5.979	-1.545	-221.2

4.5.2 Three-Layer Piezoelectric Spherical Shell

Consider a three-layer piezoelectric spherical shell with ply thicknesses $[0.4h/0.2h/0.4h]$ subjected to a localized uniform pressure symmetrically distributed on the top surface by

$$p_3^+ = -p_0 \;\text{ for }\; 0 \le \theta_1 \le \theta_0, \;\; \pi - \theta_0 \le \theta_1 \le \pi \;\text{ and }\; 0 \le \theta_2 \le 2\pi, \tag{4.40}$$

where θ_1 and θ_2 are the spherical coordinates of the middle surface; $p_0 = 1\,\mathrm{N/m^2}$ and $\theta_0 = \arccos(0.75)$. The bottom and top layers are made of the $BaTiO_3$ whereas the middle layer of the PZT-4 with the material properties given in Table 4.4 and (Dunn

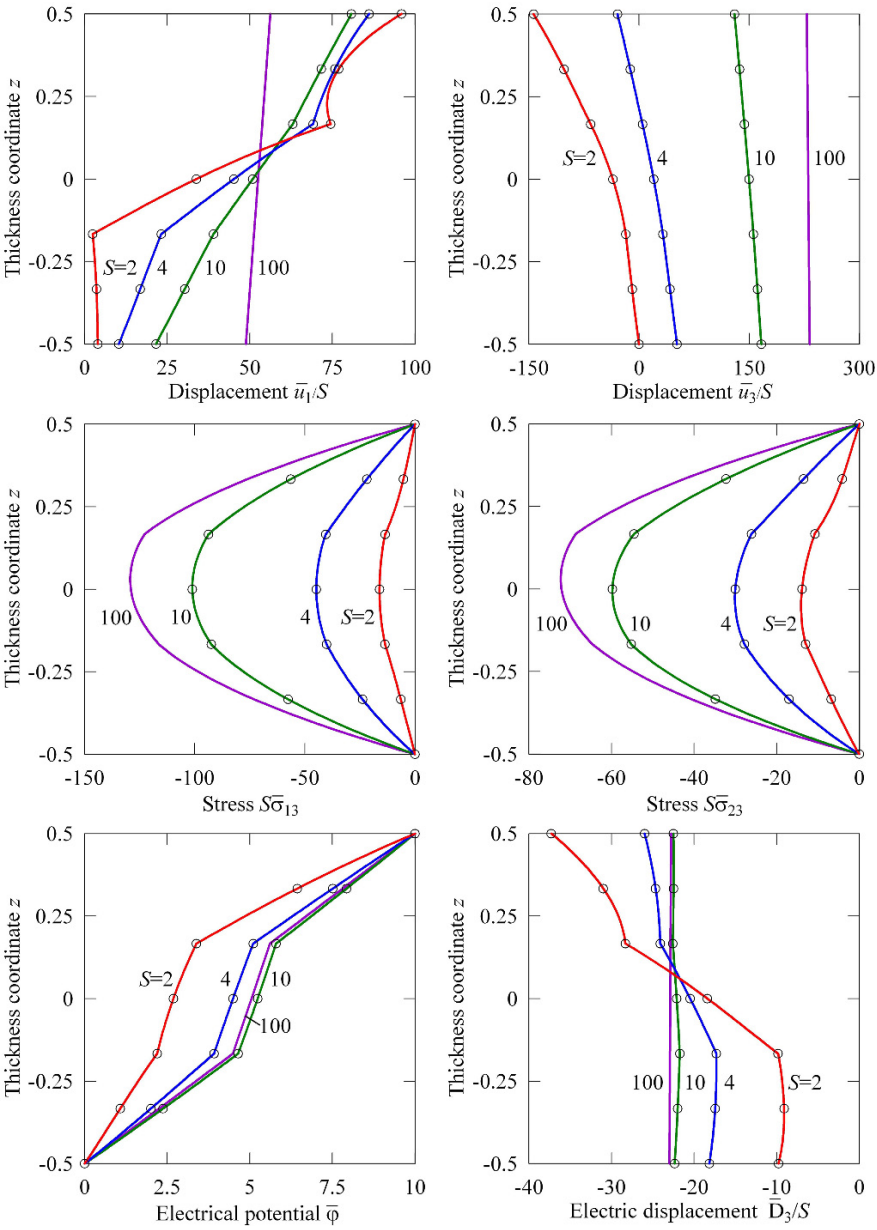

Fig. 4.5: Through-thickness distributions of displacements, transverse shear stresses, electric potential and electric displacement for a three-layer cylindrical shell subjected to electric loading for $I_1 = I_2 = I_3 = 5$: GeXPS4 element (—) and exact SaS solution (Kulikov and Plotnikova, 2013) (∘)

Table 4.5: Results for a three-layer piezoelectric spherical shell with $R/h = 1.5$

I_n	$\bar{u}_1(0.5)$	$\bar{u}_3(0.5)$	$\bar{\varphi}(0.5)$	$\bar{\sigma}_{11}(0.5)$	$\bar{\sigma}_{22}(0.5)$	$\bar{\sigma}_{13}(0)$	$\bar{\sigma}_{33}(0)$	$\bar{D}_3(0)$
3	-0.7592	-3.572	4.131	-10.98	-9.862	-0.5407	-4.367	-1.062
5	-0.7655	-3.582	4.119	-10.78	-9.725	-0.5491	-4.370	-1.097
7	-0.7655	-3.582	4.120	-10.79	-9.738	-0.5490	-4.370	-1.096
9	-0.7655	-3.582	4.120	-10.79	-9.738	-0.5490	-4.370	-1.096

and Taya, 1994). This problem is a good benchmark to test the proposed analytical integration scheme because in the literature an exact 3D solution is available (Chen et al, 2001).

Owing to symmetry, we consider a part of the shell ($\theta_* \le \theta_1 \le 90°$, $0 \le \theta_2 \le 10°$) depicted in Fig. 4.6, which is modeled by a fine mesh with 450×1 GeXPS4 elements to describe correctly the boundary conditions on external surfaces and the continuity conditions at interfaces for transverse components of stresses and electric displacement, where $\theta_* = 0.001°$. To analyze the results efficiently, we introduce the following dimensionless variables as functions of the thickness coordinate:

$$\begin{aligned}
&\bar{u}_1 = 10c_{44}u_1(\pi/6, 0, z)/RS\,p_0, \quad \bar{u}_3 = 10c_{44}u_3(\pi/6, 0, z)/RS\,p_0,\\
&\bar{\sigma}_{11} = 10\sigma_{11}(\pi/6, 0, z)/S\,p_0, \quad \bar{\sigma}_{22} = 10\sigma_{22}(\pi/6, 0, z)/S\,p_0,\\
&\bar{\sigma}_{13} = 10\sigma_{13}(\pi/6, 0, z)/p_0, \quad \bar{\sigma}_{33} = \sigma_{33}(\pi/6, 0, z)/p_0,\\
&\bar{\varphi} = 100e_{33}\varphi(\pi/6, 0, z)/Rp_0, \quad \bar{D}_3 = 10S\,c_{44}D_3(\pi/6, 0, z)/e_{33}p_0, \quad z = \theta_3/h,
\end{aligned} \tag{4.41}$$

where $S = R/h$ is the slenderness ratio; $R = 1\,\text{m}$ is the radius of the middle surface; $c_{44} = 44.0\,\text{GPa}$ and $e_{33} = 17.5\,\text{C/m}^2$ are the representative moduli.

The data listed in Table 4.5 show that the GeXPS4 element allows reproducing the 3D solution of piezoelectricity (Chen et al, 2001) for a thick spherical shell with a high accuracy by using the sufficiently large number of SaS inside the layers. Figures

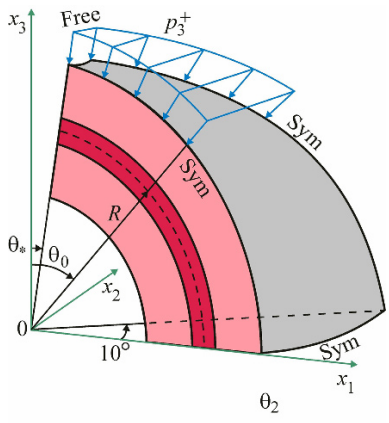

Fig. 4.6 A part of the three-layer piezoelectric spherical shell modeled by regular $k \times 1$ meshes

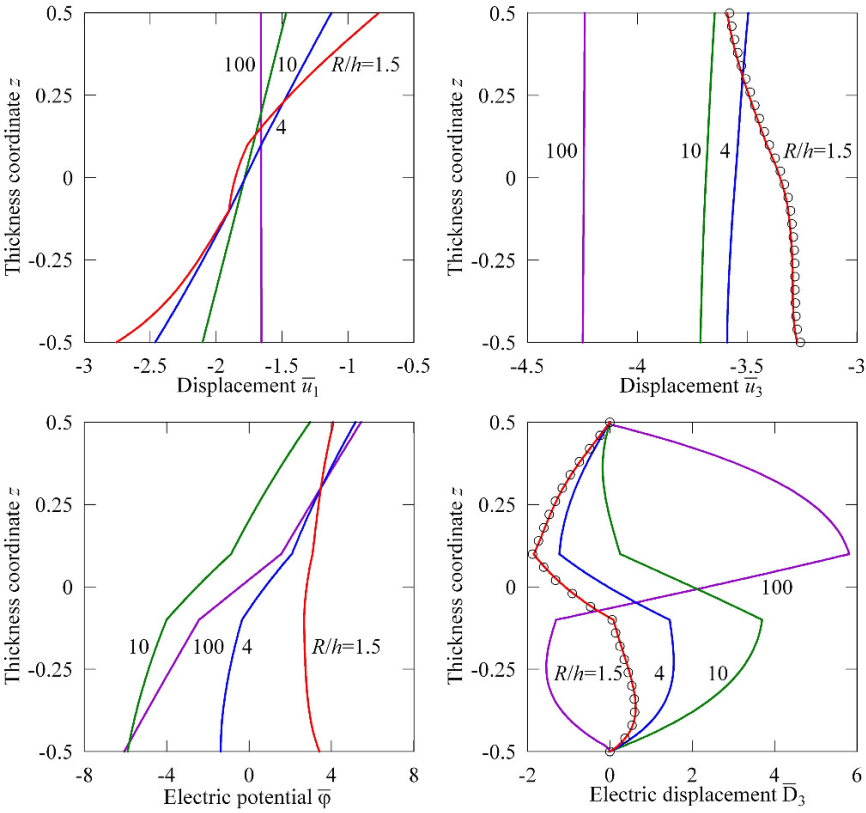

Fig. 4.7: Through-thickness distributions of displacements, electric potential and electric displacement for a three-layer piezoelectric spherical shell for $I_1 = I_2 = I_3 = 9$: GeXPS4 element (—) and exact 3D solution (Chen et al, 2001) (∘)

4.7 and 4.8 display the distributions of displacements, electric potential, electric displacement and stresses (4.41) through the thickness for various slenderness ratios by choosing nine SaS inside each layer. A comparison with the exact 3D solution (Chen et al, 2001) is also presented. One can see that the results for a thick shell are very close.

Figure 4.9 shows the results of the convergence study through the use of the normalized transverse displacement, electric potential and stresses for thick and thin shells with nine SaS for each layer. The regular $30k \times 1$ meshes are utilized with the mesh parameter k that runs from 1 to 5. The reference values for the displacement, electric potential and stresses are listed in Table 4.6. They have been obtained by using a fine 450×1 mesh. As can be seen, the GeXPS4 element demonstrates again good convergence characteristics.

Table 4.6: Reference values of basic variables for a three-layer piezoelectric spherical shell for $I_1 = I_2 = I_3 = 9$ by using a fine 450×1 mesh

S	$\bar{u}_3^{\text{ref}}(0.5)$	$\bar{\varphi}^{\text{ref}}(0.5)$	$\bar{\sigma}_{11}^{\text{ref}}(0.5)$	$\bar{\sigma}_{33}^{\text{ref}}(0)$
1.5	-3.582	4.120	-10.79	-0.5490
4	-3.486	4.607	-8.748	-0.4539
10	-3.638	2.970	-8.544	-0.4037
100	-4.239	5.429	-5.589	-0.4870

4.6 Conclusions

The paper presents a geometrically exact hybrid-mixed four-node piezoelectric solid-shell element (GeXPS4) based on the SaS formulation in which displacements and electric potentials of SaS are utilized as fundamental shell unknowns. The SaS are located at Chebyshev polynomial nodes inside the layers and interfaces as well that improves significantly the behavior of the higher-order Lagrange interpolations. To implement the efficient analytical integration throughout the element, the enhanced ANS method for all components of the strain tensor and electric field is employed. The feature of the GeXPS4 element is that the element stiffness matrices are evaluated without the use of expensive numerical matrix inversion. As a result, the GeXPS4 element exhibits a superior performance in the case of coarse mesh configurations. Therefore, it can be recommended for the 3D stress analysis of thick and thin doubly-curved shells.

Acknowledgements This work was supported by the Russian Ministry of Education and Science (Grants No. 9.1148.2017/4.6 and 9.4914.2017/6.7).

References

Bakhvalov NS (1977) Numerical Methods: Analysis, Algebra, Ordinary Differential Equations. MIR, Moscow

Bathe KJ, Dvorkin EN (1986) A formulation of general shell elements-the use of mixed interpolation of tensorial components. Int J Numer Meth Engng 22(3):697–722

Bathe KJ, Lee PS, Hiller JF (2003) Towards improving the MITC9 shell element. Comput Struct 81(8):477–489

Betsch P, Stein E (1995) An assumed strain approach avoiding artificial thickness straining for a non-linear 4-node shell element. Comm Num Meth Engng 11(11):899–909

Carrera E (1999) Multilayered shell theories accounting for layerwise mixed description. Part 1: Governing equations. AIAA J 37(9):1107–1116

Carrera E (2003) Theories and finite elements for multilayered plates and shells: A unified compact formulation with numerical assessment and benchmarking. Arch Comput Meth Engng 10(3):215–296

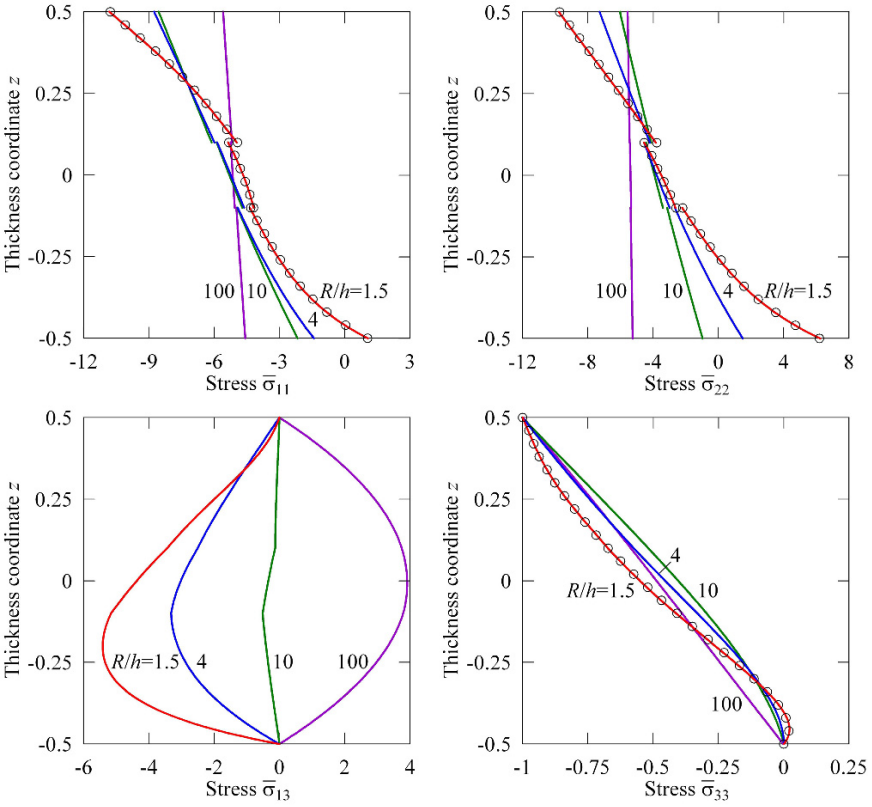

Fig. 4.8: Through-thickness distribution of stresses for a three-layer piezoelectric spherical shell for $I_1 = I_2 = I_3 = 9$: GeXPS4 element (—) and exact 3D solution (Chen et al, 2001) (∘)

Carrera E, Valvano S (2017) Analysis of laminated composite structures with embedded piezoelectric sheets by variable kinematic shell elements. J Intel Mater Systems Struct online:1–29, DOI 10.1177/1045389X17704913

Carrera E, Brischetto S, Nali P (2011) Plates and Shells for Smart Structures: Classical and Advanced Theories for Modeling and Analysis. John Wiley & Sons Ltd, Chichester

Carrera E, Cinefra M, Petrolo M, Zappino E (2014) Finite Element Analysis of Structures Through Unified Formulation. John Wiley & Sons Ltd, Chichester

Chen WQ, Ding HJ, Xu RQ (2001) Three-dimensional static analysis of multi-layered piezoelectric hollow spheres via the state space method. Int J Solids Struct 38(28):4921–4936

Cinefra M, Carrera E, Valvano S (2015) Variable kinematic shell elements for the analysis of electro-mechanical problems. Mech Adv Mater Struct 22:77–106

Dunn ML, Taya M (1994) Electroelastic field concentrations in and around inhomogeneities in piezoelectric solids. Trans ASME J Appl Mech 61(2):474–475

Heyliger P (1997) A note on the static behavior of simply supported laminated piezoelectric cylinders. Int J Solids Struct 34(29):3781 – 3794

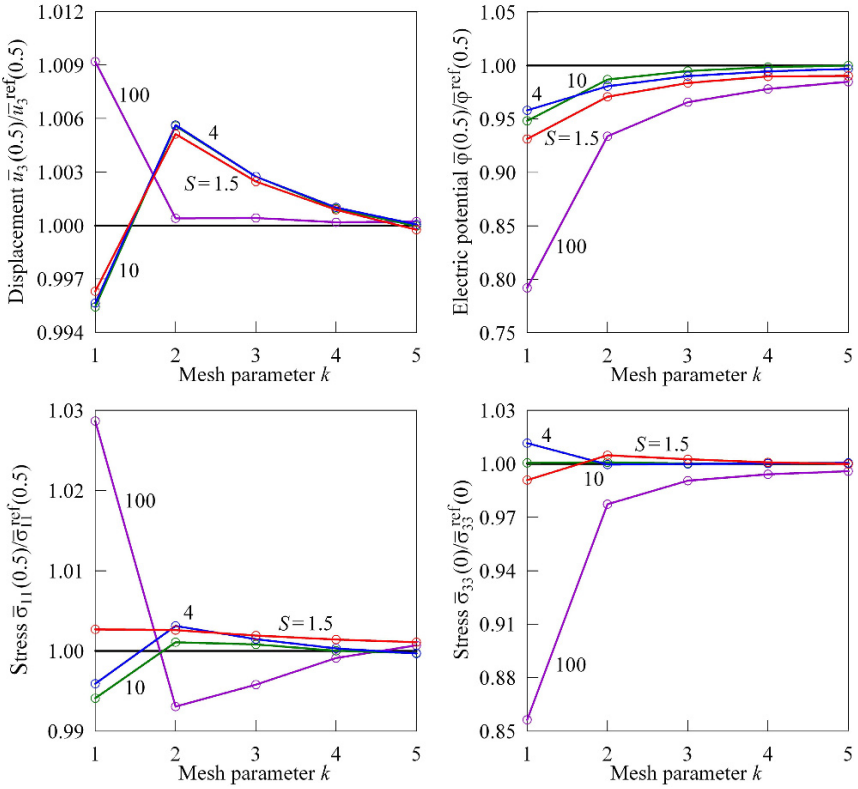

Fig. 4.9: Convergence study due to mesh refinement for a three-layer spherical shell for $I_1 = I_2 = I_3 = 9$; the reference solution (—) is provided by Table 4.6

Hughes TJR, Tezduyar TE (1981) Finite elements based upon Mindlin plate theory with particular reference to the four-node bilinear isoparametric element. Trans ASME J Appl Mech 48(3):587–596

Klinkel S, Wagner W (2006) A geometrically non-linear piezoelectric solid shell element based on a mixed multi-field variational formulation. Int J Numer Meth Eng 65(3):349–382

Klinkel S, Wagner W (2008) A piezoelectric solid shell element based on a mixed variational formulation for geometrically linear and nonlinear applications. Comp Struct 86(1):38 – 46

Ko Y, Lee PS, Bathe KJ (2017) A new MITC4+ shell element. Comput Struct 182:404–418

Kulikov GM (2001) Refined global approximation theory of multilayered plates and shells. J Eng Mech 127(2):119–125

Kulikov GM, Carrera E (2008) Finite deformation higher-order shell models and rigid-body motions. Int J Solids Struct 45(11):3153–3172

Kulikov GM, Plotnikova SV (2008) Geometrically exact four-node piezoelectric solid-shell element. Mech Adv Mater Struct 15(3-4):199–207

Kulikov GM, Plotnikova SV (2010) Solution of a coupled problem of thermopiezoelectricity based on a geometrically exact shell element. Mech Comp Mater 46(4):349–364

Kulikov GM, Plotnikova SV (2011a) Exact geometry piezoelectric solid-shell element based on the 7-parameter model. Mech Adv Mater Struct 18(2):133–146

Kulikov GM, Plotnikova SV (2011b) Finite rotation piezoelectric exact geometry solid-shell element with nine degrees of freedom per node. Comput Mater Continua 23:233–264

Kulikov GM, Plotnikova SV (2011c) Non-linear exact geometry 12-node solid-shell element with three translational degrees of freedom per node. Int J Numer Meth Engng 88(13):1363–1389

Kulikov GM, Plotnikova SV (2011d) On the use of a new concept of sampling surfaces in shell theory. In: Altenbach H, Eremeyev VA (eds) Shell-like Structures: Non-classical Theories and Applications, Springer, Berlin, Heidelberg, pp 715–726

Kulikov GM, Plotnikova SV (2013) A sampling surfaces method and its application to three-dimensional exact solutions for piezoelectric laminated shells. Int J Solids Struct 50(11):1930–1943

Kulikov GM, Plotnikova SV (2014) Exact electroelastic analysis of functionally graded piezoelectric shells. Int J Solids Struct 51(1):13–25

Kulikov GM, Plotnikova SV (2015) The use of 9-parameter shell theory for development of exact geometry 12-node quadrilateral piezoelectric laminated solid-shell elements. Mech Adv Mater Struct 22(6):490–502

Kulikov GM, Plotnikova SV (2017) Assessment of the sampling surfaces formulation for thermo-electroelastic analysis of layered and functionally graded piezoelectric shells. Mech Adv Mater Struct 24(5):392–409

Kulikov GM, Mamontov AA, Plotnikova SV (2015) Coupled thermoelectroelastic stress analysis of piezoelectric shells. Compos Struct 124:65–76

Lee S, Goo NS, Park HC, Yoon KJ, Cho C (2003) A nine-node assumed strain shell element for analysis of a coupled electro-mechanical system. Smart Mater Struct 12:355–362

Lentzen S (2009) Nonlinearly coupled thermopiezoelectric modelling and FE-simulation of smart structures. No. 419 in Fortschritt-Berichte VDI, Reihe 20, VDI-Verlag GmbH, Düsseldorf

Macneal RH (1982) Derivation of element stiffness matrices by assumed strain distributions. Nuclear Engineering and Design 70(1):3–12

Park KC, Stanley GM (1986) A curved C^0 shell element based on assumed natural-coordinate strains. Trans ASME J Appl Mech 53(2):278–290

Sze KY, Yao LQ (2000) A hybrid stress ANS solid-shell element and its generalization for smart structure modelling. Part I: Solid-shell element formulation. Int J Numer Meth Eng 48:545–564

Sze KY, Yao LQ, Yi S (2000) A hybrid stress ANS solid-shell element and its generalization for smart structure modelling. Part II: Smart structure modelling. Int J Numer Meth Eng 48:565–582

Zheng S, Wang X, Chen W (2004) The formulation of a refined hybrid enhanced assumed strain solid shell element and its application to model smart structures containing distributed piezoelectric sensors/actuators. Smart Mater Struct 13:N43–N50